The Astrophysical Journal, 752:91 (7pp), 2012 June 20 doi:10.1088/0004-637X/752/2/91

CO $J = 2$–1 LINE EMISSION IN CLUSTER GALAXIES AT $z \sim 1$: FUELING STAR FORMATION IN DENSE ENVIRONMENTS*

Jeff Wagg[1], Alexandra Pope[2], Stacey Alberts[2], Lee Armus[3], Mark Brodwin[4], Robert S. Bussmann[5], Vandana Desai[3], Arjun Dey[6], Buell Jannuzi[6], Emeric Le Floc'h[7], Jason Melbourne[8], and Daniel Stern[9]
[1] European Southern Observatory, Casilla 19001, Santiago, Chile; jwagg@eso.org
[2] Department of Astronomy, University of Massachusetts, Amherst, MA 01003, USA
[3] Spitzer Science Center, California Institute of Technology, MS 220-6, Pasadena, CA 91125, USA
[4] Department of Physics, University of Missouri, 5110 Rockhill Road, Kansas City, MO 64110, USA
[5] Harvard-Smithsonian Center for Astrophysics, 60 Garden Street, Cambridge, MA 02138, USA
[6] National Optical Astronomy Observatory, Tucson, AZ 85726-6732, USA
[7] AIM, CNRS, Université Paris Diderot, Bât. 709, CEA-Saclay, 91191 Gif-sur-Yvette Cedex, France
[8] California Institute of Technology, Pasadena, CA 91125, USA
[9] Jet Propulsion Laboratory, California Institute of Technology, Pasadena, CA 91109, USA
Received 2012 February 3; accepted 2012 April 12; published 2012 May 30

ABSTRACT

We present observations of CO $J = 2$–1 line emission in infrared-luminous cluster galaxies at $z \sim 1$ using the IRAM Plateau de Bure Interferometer. Our two primary targets are optically faint, dust-obscured galaxies (DOGs) found to lie within 2 Mpc of the centers of two massive ($>10^{14}\ M_\odot$) galaxy clusters. CO line emission is not detected in either DOG. We calculate 3σ upper limits to the CO $J = 2$–1 line luminosities, $L'_{\rm CO} < 6.08 \times 10^9$ and $<6.63 \times 10^9$ K km s^{-1} pc^2. Assuming a CO-to-H$_2$ conversion factor derived for ultraluminous infrared galaxies in the local universe, this translates to limits on the cold molecular gas mass of $M_{\rm H_2} < 4.86 \times 10^9\ M_\odot$ and $M_{\rm H_2} < 5.30 \times 10^9\ M_\odot$. Both DOGs exhibit mid-infrared continuum emission that follows a power law, suggesting that an active galactic nucleus (AGN) contributes to the dust heating. As such, estimates of the star formation efficiencies in these DOGs are uncertain. A third cluster member with an infrared luminosity, $L_{\rm IR} < 7.4 \times 10^{11}\ L_\odot$, is serendipitously detected in CO $J = 2$–1 line emission in the field of one of the DOGs located roughly two virial radii away from the cluster center. The optical spectrum of this object suggests that it is likely an obscured AGN, and the measured CO line luminosity is $L'_{\rm CO} = (1.94 \pm 0.35) \times 10^{10}$ K km s^{-1} pc^2, which leads to an estimated cold molecular gas mass $M_{\rm H_2} = (1.55 \pm 0.28) \times 10^{10}\ M_\odot$. A significant reservoir of molecular gas in a $z \sim 1$ galaxy located away from the cluster center demonstrates that the fuel can exist to drive an increase in star formation and AGN activity at the outskirts of high-redshift clusters.

Key words: galaxies: clusters: general – galaxies: evolution – galaxies: formation – ISM: molecules

Online-only material: color figure

1. INTRODUCTION

In the local universe, the average star formation rate (SFR) in galaxies depends on the local environment, decreasing with increasing galaxy space density (e.g., Lewis et al. 2002; Kauffmann et al. 2004). Recent studies have demonstrated that the average SFR in galaxies in rich environments is much higher at $z \sim 1$ than it is locally (Elbaz et al. 2007; Cooper et al. 2008), suggesting that galaxies in $z \gtrsim 1$ clusters exhibit more intense star formation than their analogs in the local universe. Indeed, the average SFR in galaxies is higher in massive clusters at these redshifts (Tran et al. 2010; Hilton et al. 2010; M. Brodwin et al., in preparation). Furthermore, the number of cluster galaxies with an active galactic nucleus (AGN) has been found to increase out to redshifts $z > 1$ (e.g., Galametz et al. 2009; Martini et al. 2009). At intermediate redshifts, recent studies have found that luminous infrared galaxies (LIRGs) are preferentially forming stars at the outskirts of some massive clusters (e.g., Haines et al. 2010), suggesting that star formation may be quenched within the central regions at these epochs. This star formation and AGN activity in high-redshift cluster galaxies should be fueled by significant reservoirs of molecular gas, and observations of this gas can provide insight into the processes governing galaxy formation in dense environments.

The most effective means of studying the molecular gas in high-redshift galaxies is through observations of redshifted CO line emission (see reviews by Solomon & Vanden Bout 2005; Carilli et al. 2011b), as the luminosity in the lowest-J CO line transitions ($J = 2$–1 or $J = 1$–0) provides an estimate of the total mass in cold molecular gas. Sensitive interferometric imaging of CO line emission redshifted to millimeter and centimeter wavelengths has been used to probe the molecular gas content of members of galaxy overdensities at redshifts $z > 2$ (e.g., Nesvadba et al. 2009; Riechers et al. 2010; Carilli et al. 2011a). These observations revealed that gas-rich galaxies do reside in proposed galaxy overdensities at high redshift, presumably fueling starburst and AGN activity in objects that are rapidly evolving toward massive galaxies at $z \sim 0$. In the nearby universe, most early-type galaxies inhabiting rich clusters are gas-poor (e.g., Combes et al. 2007), as the cold gas has been consumed during star formation, or removed through processes such as ram pressure stripping. At intermediate redshifts, CO $J = 1$–0 line emission has been detected in two LIRGs found within 2–3 virial radii of the center of the rich cluster Cl 0024+16 at $z = 0.395$ (Geach et al. 2009). It is possible that such systems will consume their gas rapidly as they enter the cluster. However,

* Based on observations carried out with the IRAM Plateau de Bure Interferometer. IRAM is supported by INSU/CNRS (France), MPG (Germany), and IGN (Spain).

Table 1
Observed Properties of $z \sim 1$ Cluster Galaxies

Source	z	$S_{24\,\mu\mathrm{m}}$ (mJy)	L_{IR} (8–1000 μm) ($L_\odot$)	L_{FIR} (40–500 μm) ($L_\odot$)	$\log(M_*)$[a] ($M_\odot$)	$\nu_{\mathrm{CO2-1}}$ (GHz)	rms[b] (mJy)	L'_{CO} (K km s^{-1} pc^2)
DOG1	1.1160	2.92 ± 0.07	$<2.8 \times 10^{12}$[c]	$<1.6 \times 10^{12}$[c]	10.57 ± 0.14	108.950	0.70	$<6.08 \times 10^{9}$[d]
DOG2	1.2405	1.67 ± 0.05	$<1.7 \times 10^{12}$[c]	$<5.8 \times 10^{11}$[c]	10.94 ± 0.13	102.896	0.62	$<6.63 \times 10^{9}$[d]
COserendip	1.1147 (CO)	0.45 ± 0.04	$<7.4 \times 10^{11}$[c]	$<4.9 \times 10^{11}$[c]	10.97 ± 0.14	109.018	0.66	$(1.94 \pm 0.35) \times 10^{10}$

Notes.
[a] The uncertainties on M_* are for the specific choice of star formation history and initial mass function, and therefore underestimate the uncertainty in the absolute values.
[b] The quoted rms noise values are calculated for a velocity resolution of 100 km s^{-1}.
[c] Upper limits to the infrared and far-infrared luminosities are due to source blending, or non-detections in the SPIRE submillimeter bands.
[d] 3σ upper limits assuming a 300 km s^{-1} CO line width.

these clusters are still at relatively low redshift, in the regime where we expect star formation activity to be suppressed in the harsh cluster environments. To date, there have been no studies of the cold molecular gas traced by redshifted CO line emission in massive ($>10^{14}\,M_\odot$) galaxy clusters at $z > 1$.

The formation of massive galaxies at high redshift is often traced by strong infrared emission, which probes an active phase of dust-obscured star formation and AGN activity, such as that seen in ultraluminous infrared galaxies (ULIRGs) in the nearby universe. Local and high-redshift ULIRGs are invariably observed to be rich in molecular gas which provides fuel for ongoing star formation activity (Solomon & Vanden Bout 2005). One method used to identify ULIRGs at high redshift is through a high mid-infrared-to-optical flux density ratio, which has been used to reveal a population of $z \sim 1$–3 dust-obscured galaxies (DOGs; Dey et al. 2008; Fiore et al. 2008) which are strongly clustered (Brodwin et al. 2008). DOGs have high estimated IR luminosities, $L_{\mathrm{IR}} = 10^{12}$–$10^{13}\,L_\odot$, that are likely powered by a combination of star formation and AGN activity (Dey et al. 2008; Desai et al. 2009), and theoretical models of merging galaxies are able to reproduce many of the observed properties of DOGs (Narayanan et al. 2010). The significant SFRs of starburst-dominated DOGs implied by their FIR luminosities (SFR $> 500\,M_\odot$ yr^{-1}) are expected to be fueled by large masses of molecular gas. We find that some of the DOGs lie within 1–2 Mpc of the centers of massive, high-redshift galaxy clusters from the IRAC Shallow Cluster Survey (ISCS; Eisenhardt et al. 2008). These clusters have masses $> 10^{14}\,M_\odot$ (Brodwin et al. 2011; Jee et al. 2011), estimated from weak lensing and X-ray observations. The DOGs in these clusters provide excellent targets for studying the gas properties of infrared-luminous galaxies residing in the densest environments at $z > 1$.

In the present work, we use the IRAM Plateau de Bure Interferometer (PdBI) to conduct a sensitive search for CO $J = 2$–1 line emission in two DOGs associated with massive galaxy clusters at $z > 1$ in order to measure their total cold molecular gas masses and study the star formation efficiency of galaxies in extreme cluster environments. Throughout this analysis, we adopt a cosmological model with $(\Omega_\Lambda, \Omega_m, h) = (0.73, 0.27, 0.71)$ (Spergel et al. 2007). At a redshift of $z = 1.2$, the angular scale is 8.346 kpc/$''$.

2. OUR TARGETS

Dey et al. (2008) identify 2603 DOGs in the NOAO Deep Wide Field Survey of the 9 deg^2 Boötes field (Jannuzi & Dey 1999). This field contains a sample of over 20 massive galaxy clusters spectroscopically confirmed to lie at $z > 1$ (Stanford et al. 2005; Elston et al. 2006; Brodwin et al. 2006, 2011; Eisenhardt et al. 2008). Three DOGs with spectroscopic redshifts are found to lie within a distance of 2 Mpc from the centers of these known clusters. This separation places them close to their expected virial radii given the estimated masses of these clusters ($\gtrsim 10^{14}\,M_\odot$; Jee et al. 2011). Of the three DOGs associated with clusters, the 24 μm flux densities predict that two of these should have infrared luminosities, $L_{\mathrm{IR}} \gtrsim 10^{12}\,L_\odot$, making them suitably bright for millimeter-wavelength observations of CO line emission. SST24 J143234.9+333637 (hereafter "DOG1") lies at a projected separation of ∼2 Mpc from the center of cluster ISCS J1432.4+3332 ($r_{200} = 1.06^{+0.11}_{-0.09}$), and SST24 J143430.6+342757 (hereafter "DOG2") is at a projected separation of ∼0.8 Mpc from the center of cluster ISCS J1434.5+3427 ($r_{200} = 0.82^{+0.19}_{-0.14}$). Both DOG1 and DOG2 have optical spectroscopic redshifts (Table 1). All source names indicate J2000 coordinates. The shape of the mid-infrared spectral energy distributions (SEDs) of DOG1 and DOG2 can be described by a power law, indicating that AGNs are present (Stern et al. 2005; Dey et al. 2008). The optical Keck/LRIS spectra of DOG1 reveal that this object is a type-2 AGN at $z = 1.1160$. Narrow, high-ionization lines of Ne are clearly detected, as well as He II and C III]. The Keck/DEIMOS optical spectrum of DOG2 shows [O II] emission at $z = 1.2405$, with low signal-to-noise ratio detections of corresponding Ca II HK absorption and a 4000 Å break. The optical spectrum shows no high-ionization lines indicative of an active galaxy. Independent of whether the AGN or star formation is the dominant source of their infrared luminosities, we expect the DOGs to have significant masses of cold molecular gas, as is typically found in objects whose dusty interstellar medium is strongly irradiated.

Optical-to-submillimeter wavelength images for each of our two target fields are shown in Figure 1. In order to better interpret the CO observations of our targets, we fit the available infrared photometry with SED templates to estimate their infrared (8–1000 μm) and far-infrared (40–500 μm) luminosities. Publicly available *Herschel*/SPIRE data now exist for both targets in Boötes from the HerMES survey (Oliver et al. 2010). We reprocessed the SPIRE maps to remove striping, astrometry offsets, and glitches before performing our own photometry measurements on the images at 250, 350, and 500 μm. DOG2 is formally undetected in the SPIRE bands while DOG1 and a second 24 μm source (SST24 J143235.8+333632—described in Section 4.2) are both part of a group of 24 μm sources which are blended together as a single source in the lower resolution SPIRE maps, highlighted by the 250 μm image shown in Figure 1. We measure the SPIRE flux densities at the exact position of the 24 μm counterparts, noting that the resulting infrared luminosities should be considered upper limits, since

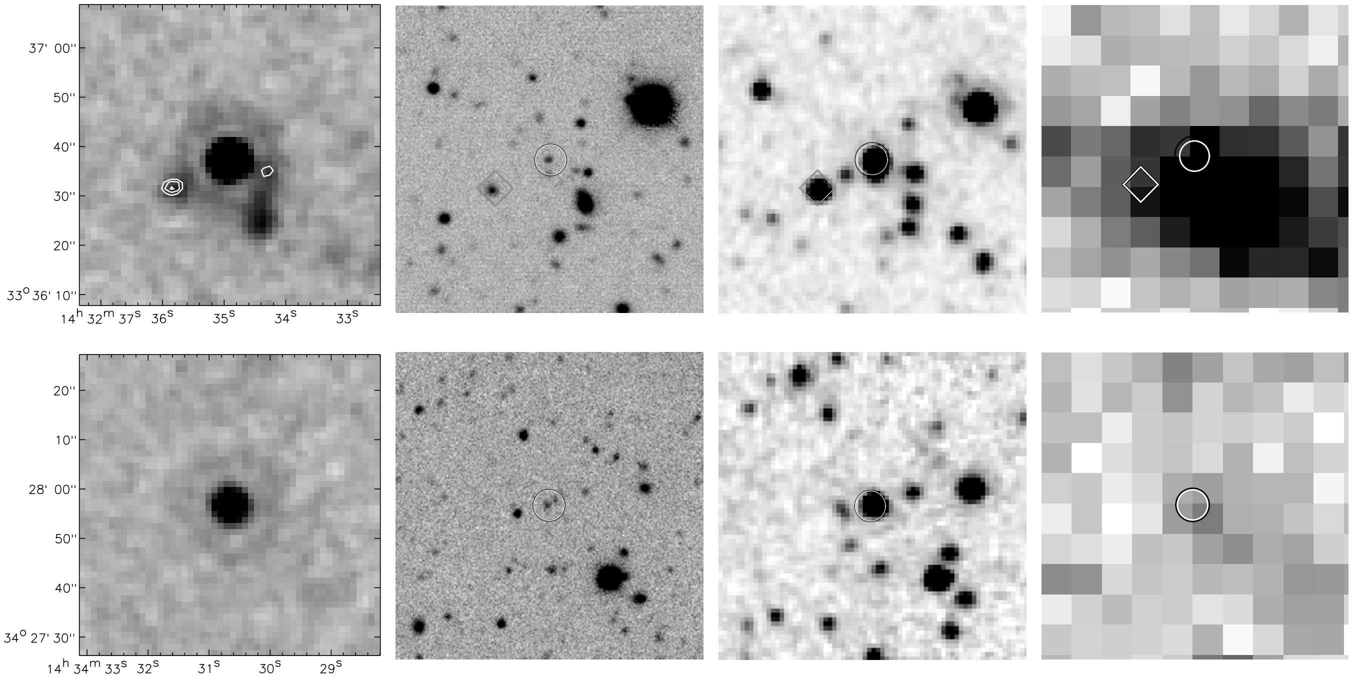

Figure 1. Images of the DOG1 (top) and DOG2 (bottom) fields. From left to right are shown $1' \times 1'$ images at 24 μm, R band, 4.5 μm, and SPIRE 250 μm. The circles denote the positions of the two DOGs studied here, while the diamond indicates the position of the CO-detected source we refer to as COserendip. Overlaid on the 24 μm image of the DOG1 and COserendip field are CO intensity contour levels of $(3, 4, 5) \times \sigma$, where $\sigma = 0.27$ mJy per 500 km s^{-1} channel.

there may be a significant contribution from the nearby blended sources. We fit the photometry using the new starburst and AGN SED templates of A. Kirkpatrick et al. (ApJ, submitted) which are developed using a complete suite of data for high-redshift galaxies including IRS spectroscopy, *Spitzer* imaging from 3.6 to 70 μm, and *Herschel* imaging from 100 to 500 μm. The resulting luminosities are listed in Table 1. Both DOG1 and DOG2 exhibit mid-infrared continuum emission that can be described by a power law, suggesting that AGNs are present. However, the current data prohibit us from determining if star formation or AGN activity dominates the far-infrared luminosities.

Using broadband optical through near-IR photometry, we constrain the stellar masses of our targets. High signal-to-noise detections at each of B_W, R, I, J, H, and Ks bands (Jannuzi & Dey 1999; A. H. Gonzalez et al., in preparation) were fitted with synthesized stellar population models following the procedure described in Bussmann et al. (2012), where the best-fit stellar mass, M_*, and the 1σ uncertainties are determined by marginalizing over stellar population age and reddening. Detections of these objects in the IRAC bands (Ashby et al. 2009) were not used in the fitting. A simple stellar population is assumed, as well as a Chabrier initial mass function (Chabrier 2003), and the Bruzual & Charlot (2003) synthesis models. The best-fit stellar masses and their 1σ uncertainties (for the given choice of star formation history and initial mass function) are listed in Table 1. More complex star formation histories can lead to an increase in these stellar mass estimates of up to ∼0.5 dex (Bussmann et al. 2012).

3. OBSERVATIONS AND DATA ANALYSIS

3.1. PdBI Observations of CO $J = 2$–1 Line Emission

At the redshifts of DOG1 and DOG2, the 230.538 GHz CO $J = 2$–1 line is redshifted to 108.950 and 102.896 GHz, which is accessible with the 3 mm band receivers on the PdBI. Observations were made with five antennas of the PdBI on four dates between 2010 August 29 and October 3, while the array was in the compact 5Dq configuration. A total of 12.7 hr (including overheads) was spent observing DOG1, while another 10 hr was spent observing the DOG2 field. The correlator was set up to sample 3.6 GHz of bandwidth in two polarizations, covering 9880 and 10,460 km s^{-1} at these frequencies. With such a large bandwidth and a field of view of ∼0.5 arcmin^2, we are also able to conduct a serendipitous search for CO $J = 2$–1 line emission in additional cluster members. The lowest spectral resolution mode of the correlator was adopted, and the calibrated data were resampled to a resolution of 40.1 MHz. 1749+096 and 1424+366 were observed for complex gain calibration, while observations of MWC349 and 3C345 were used to calibrate the flux density and spectral bandpass. After these observations were made, a hardware problem was uncovered by the IRAM staff which would have affected the phases on antenna 5 baselines for observations taken during our October 3 observations of DOG2. After checking these data, we do not find any clear evidence for problems with the phases, which were likely negated due to the close proximity of our phase calibrator to the target field (1424+366; $\theta \sim 2\overset{\circ}{.}5$).

Data were calibrated using the IRAM GILDAS[10] *CLIC* software package, while the imaging was performed with GILDAS *mapping*. Natural weighting was used in the imaging, and the final synthesized beam sizes are $5\overset{''}{.}0 \times 3\overset{''}{.}8$ in the DOG1 image, and $4\overset{''}{.}9 \times 3\overset{''}{.}9$ in the DOG2 image. The image map sizes are $32\overset{''}{.}0 \times 32\overset{''}{.}0$, chosen to include a significant fraction of the field of view defined by the primary beam. The calibrated *uv* data are also processed separately by a routine written by the IRAM staff that searches for emission features in the spectral line data cubes. We identify one source of significant emission (5.5σ) at $\sim 12''$ from the center of the DOG1 map, and this object is described in Section 4.2. Due to its distance from the center of the image, the flux density has been corrected for the primary

[10] http://www.iram.fr/IRAMFR/GILDAS

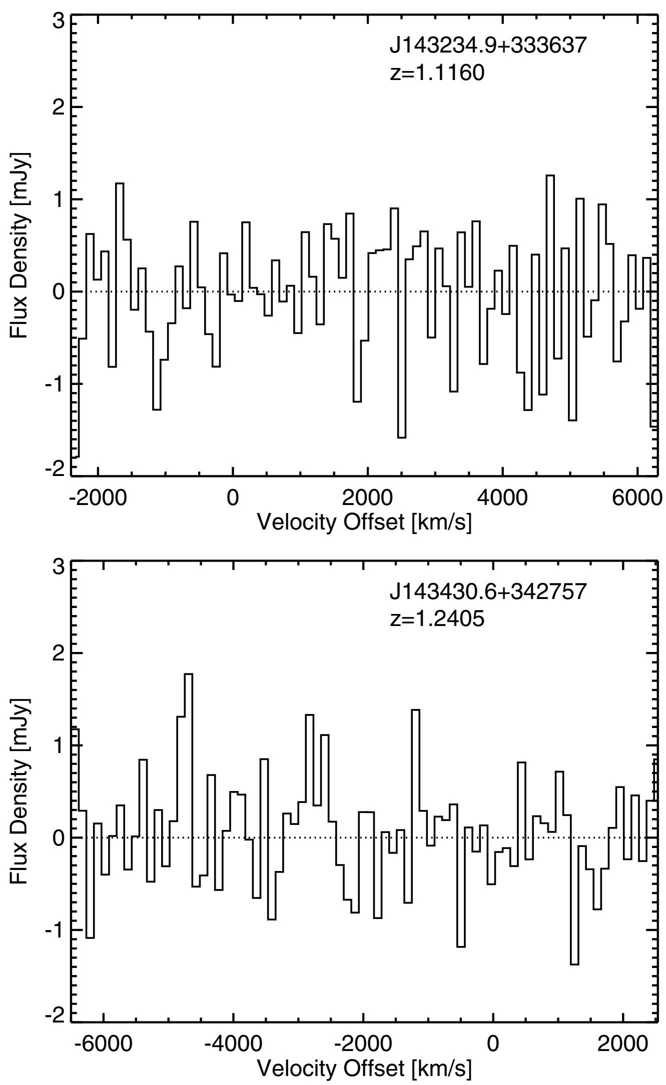

Figure 2. PdBI 3 mm band spectra at the expected redshifts of CO $J = 2$–1 line emission in DOG1 (top) and DOG2 (bottom). Velocity offsets are relative to $z = 1.1160$ for DOG1 and $z = 1.2405$ for DOG2. The spectra have been resampled to 40.1 MHz resolution, corresponding to 110.1 and 116.5 km s^{-1}. At this spectral resolution, the rms is 0.67 and 0.57 mJy, respectively.

beam by a factor of 1.033. We have verified that the detection remains after excluding a small subset of antenna 5 data that are potentially affected by a hardware problem.

4. RESULTS

4.1. CO $J = 2$–1 Line Emission in DOGs

We do not detect CO $J = 2$–1 line emission or 3 mm continuum emission in either of the DOGs (Figure 2). Table 1 lists the rms sensitivity of the spectra, calculated for a channel width of 100 km s^{-1}. We can calculate upper limits to the CO $J = 2$–1 line luminosity following the definition given by Solomon & Vanden Bout (2005):

$$L'_{\rm CO} = 3.25 \times 10^7\, S_{\rm CO}\Delta V\, \nu_{\rm obs}^{-2}\, D_L^2\, (1+z)^{-3}\ [\rm K\, km\, s^{-1}\, pc^2], \quad (1)$$

where D_L is the luminosity distance (Mpc), $\nu_{\rm obs}$ is the frequency of observation (GHz), and in the case of a non-detection, $S_{\rm CO}\Delta V$ is the 3σ upper limit to the integrated intensity (Jy km s^{-1}), defined as $3 \cdot \sqrt{\Delta V_{\rm FWHM}/\Delta V_{\rm chan}} \cdot \sigma_{\rm chan}\Delta V_{\rm chan}$. The rms in a channel of width $\Delta V_{\rm chan}$ (km s^{-1}) is given by $\sigma_{\rm chan}$ (Jy), and $\Delta V_{\rm FWHM}$ (km s^{-1}) is the assumed line width. For DOG1 and DOG2, we calculate 3σ upper limits to the CO $J = 2$–1 line luminosity, $L'_{\rm CO} < 6.08 \times 10^9$ K km s^{-1} pc^2 and $<6.63 \times 10^9$ K km s^{-1} pc^2, respectively, assuming a CO line width of 300 km s^{-1}, typical of luminous infrared quasar host galaxies at high redshift (e.g., Carilli & Wang 2006). The line width assumed for these calculations is narrower than that observed in high-redshift submillimeter galaxies (SMGs, $\sim$800 km s^{-1}; Greve et al. 2005), and we note that our upper limits to the line luminosity would increase by $\sim$60% if we were to assume the broader CO line width.

In order to convert the limits on the CO $J = 2$–1 line luminosities to molecular gas mass estimates, we first assume that the CO $J = 1$–0 and CO $J = 2$–1 lines are in thermal equilibrium, so that the luminosity in these two transitions is the same. This is the case for BzK-selected star-forming galaxies at $z \sim 1.5$ (Daddi et al. 2008; Dannerbauer et al. 2009; Aravena et al. 2010). To convert the CO line luminosity to a molecular hydrogen gas mass estimate, we adopt the conversion factor determined for nearby ULIRGs, $\alpha_{\rm CO} \sim 0.8\, M_\odot$ (K km s^{-1} pc^2)$^{-1}$ (Downes & Solomon 1998), as this is also the value generally assumed for FIR-luminous, high-redshift SMGs and quasar host galaxies. We note that the conversion factor is believed to be $\sim$5$\times$ greater for quiescent galaxies like the Milky Way (Solomon & Barrett 1991), but the presence of a mid-infrared-luminous AGN in the DOGs would favor the lower value. Adopting this conversion factor yields 3σ upper limits to the molecular gas mass, $M_{\rm H_2} < 4.86 \times 10^9\, M_\odot$ (DOG1) and $M_{\rm H_2} < 5.30 \times 10^9\, M_\odot$ (DOG2). The estimated molecular gas masses are consistent with what is observed in ULIRGs in the local universe (e.g., Downes & Solomon 1998), but roughly an order of magnitude lower than in high-redshift SMGs (e.g., Greve et al. 2005).

4.2. Serendipitous Detection of CO $J = 2$–1 Line Emission in a Cluster Member

Given that the DOGs reside in clusters, and the large bandwidth (3.6 GHz) and field of view ($\sim$46″ diameter) covered by these observations, it is possible to search the spectral line data cubes for CO $J = 2$–1 line emission from other cluster members. We detect one object in CO $J = 2$–1 line emission, $\sim$12″ to the southeast of DOG1, which we hereafter refer to as SST24 J143235.8+333632 or "COserendip" (Figure 3). At this position, there is a cluster member with a measured optical spectroscopic redshift of $z_{\rm opt} = 1.114 \pm 0.001$, determined from the [O II] line (Figure 4). The presence of C III] line emission, as well as the tentative detection of [Ne V], suggests a type-2 AGN, while a high [Ne III]-to-[O II] intensity ratio also supports the classification of COserendip as an obscured AGN (e.g., Villar-Martín et al. 2008). The CO $J = 2$–1 line emission detected in this object is offset from the optical redshift of DOG1 by approximately -200 km s^{-1}, corresponding to a redshift of $z_{\rm CO} = 1.1147$, in good agreement with the redshift of the optical counterpart. The integrated intensity of this line is $S_{\rm CO}\,\Delta V = 1.16 \pm 0.21$ Jy km s^{-1}. Although the line emission is formally detected at 5.5σ, the parameters of a Gaussian profile fit to the line are not well constrained, with a best-fit peak flux density $S_p = 2.3 \pm 0.7$ mJy and line full width at half-maximum $\Delta V_{\rm FWHM} = 447 \pm 158$ km s^{-1}. We estimate the infrared and FIR luminosities for COserendip using the best-fit SED (Figure 4), which is that of a Seyfert 2 galaxy taken from the SWIRE templates of Polletta et al. (2007). The broad width

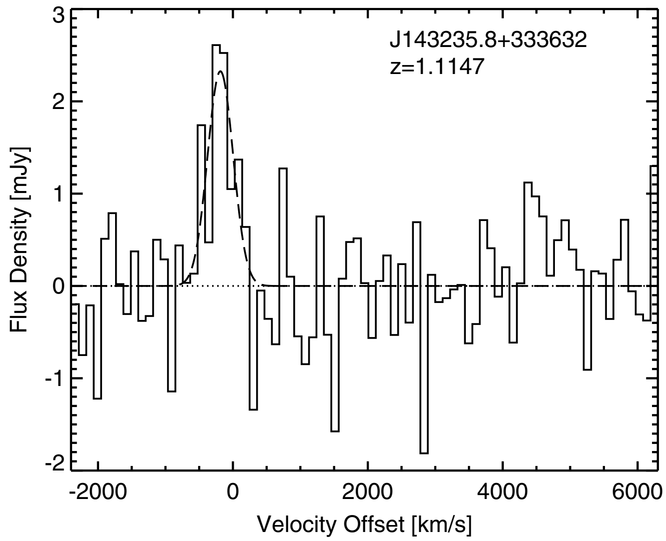

Figure 3. PdBI 3 mm band spectrum of CO $J = 2$–1 line emission in the source serendipitously detected in the DOG1 image, referred to here as COserendip. Velocity offsets are relative to $z = 1.1160$ (the optical redshift of DOG1), and the spectrum has been resampled to 40.1 MHz resolution, corresponding to 110.1 km s^{-1}. At this spectral resolution the rms is 0.63 mJy. The CO redshift for this object is $z_{\rm CO} = 1.1147$. The dashed line shows the best-fit Gaussian profile with peak flux density $S_p = 2.3 \pm 0.7$ mJy and line width $\Delta V_{\rm FWHM} = 447 \pm 158$ km s^{-1}.

of the CO line could be an indication that the molecular gas is rotating in a massive circumnuclear disk. Such broad line widths are common in the high-redshift SMG population (e.g., Greve et al. 2005), and the FIR-luminous quasar host galaxy population at $z \sim 6$ (Wang et al. 2010).

The integrated intensity of the CO $J = 2$–1 line emission in COserendip can be converted to a CO line luminosity following Equation (1), so that $L'_{\rm CO} = (1.94 \pm 0.35) \times 10^{10}$ K km s^{-1} pc^2. Following Kennicutt (1998), the infrared luminosity in COserendip implies an SFR $\leqslant 150\,M_\odot$ yr^{-1}, which is an upper limit due to the unknown contribution from the AGN. If the CO line emission were associated with a circumnuclear disk, then it would argue that the molecular gas clouds are not likely in a virialized state, motivating the adoption of the ULIRG conversion factor of Downes & Solomon (1998) to estimate the total molecular gas mass. Assuming thermalized CO $J = 2$–1 line emission, we estimate $M_{\rm H_2} = (1.55 \pm 0.28) \times 10^{10}\,M_\odot$, which is comparable to the typical mass of gas in bright, blank-field SMGs and FIR-luminous quasar host galaxies at high redshift.

5. DISCUSSION

The dust heating which gives rise to the infrared luminosities in DOG1 and DOG2 has a contribution from AGN activity, as indicated by the SED template fits showing that the mid-infrared emission in both objects can be described by a power law. Although the AGN can boost the total infrared luminosity, the scatter in the $L_{\rm IR}$-to-$L'_{\rm CO}$ ratio for nearby LIRGs and ULIRGs is large, even between those galaxies which do not contain a luminous AGN (e.g., Solomon et al. 1997). Considering the longer wavelength FIR emission, our 3σ upper limits to $L_{\rm FIR}$ are also in broad agreement with the limits on the CO $J = 2$–1 line luminosities given the observed scatter in the $L_{\rm FIR}$–$L'_{\rm CO}$ relation for nearby and high-redshift ULIRGs and more quiescent star-forming galaxies, independent of whether or not infrared-luminous quasars are included in this relation

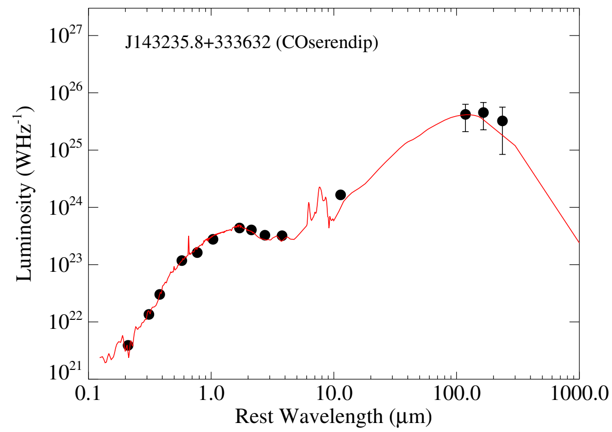

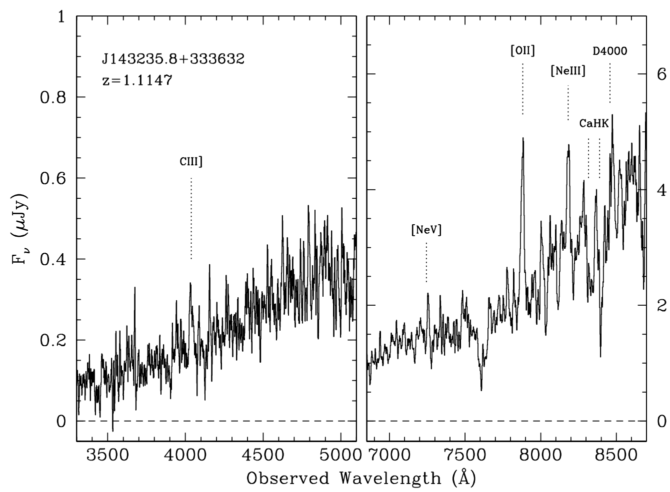

Figure 4. Top: optical through submillimeter-wavelength photometry of J143235.8+333632 (COserendip) at $z = 1.1147$. The template spectral energy distribution is that of a redshifted Seyfert 2 galaxy from the SWIRE templates of Polletta et al. (2007). Bottom: optical spectrum of COserendip, obtained with Keck/LRIS on UT 2005 June 3. The position of this target on the slitmask left a large, ∼2000 Å, gap between the blue and red arms of the dual-beam spectrograph, plotted separately above. Observations totaled 2.5 hr in clear conditions and 0$''$.9 seeing. The spectrum shows a clear detection of narrow C III] emission, as well as strong [O II] and [Ne III], suggesting that this is a type-2 AGN in the galaxy cluster. The spectrum also shows more typical features of evolved, early-type galaxies, including Ca II H + K absorption and the D4000 continuum break. The [Ne V] line emission is tentatively detected.

(A color version of this figure is available in the online journal.)

(e.g., Solomon & Vanden Bout 2005; Riechers et al. 2006; Daddi et al. 2008). As such, it is not clear whether the molecular gas content of these two DOGs found at the outskirts of massive clusters has been affected by the cluster environment. More sensitive observations of redshifted CO line emission with the Atacama Large Millimeter Array would determine if these two objects deviate from the $L_{\rm FIR}$–$L'_{\rm CO}$ relation.

The ratio of the FIR luminosity to the total molecular gas mass in a galaxy provides a measure of its star formation efficiency (SFE $= L_{\rm FIR}/M_{\rm H_2}$). In high-redshift FIR-luminous quasar host galaxies, the average star formation efficiency is SFE $\sim 430\,L_\odot\,M_\odot^{-1}$ (e.g., Solomon & Vanden Bout 2005). For ULIRGs in the local universe, the star formation efficiency is generally a factor of ∼4× higher than in more quiescent galaxies like the Milky Way (e.g., Bouché et al. 2007), and consistent with that in high-redshift SMGs ($\gtrsim 100\,L_\odot\,M_\odot^{-1}$; e.g., Frayer et al. 2011). In the case of DOG1 and DOG2, we have only upper limits to the FIR and CO line luminosities, and so are unable to estimate meaningful star formation efficiencies for these objects. In the case of COserendip, the SED template fitting indicates $L_{\rm FIR} < 4.9 \times 10^{11}\, L_\odot$, and so we estimate that the star formation efficiency is SFE $< 32\, L_\odot\, M_\odot^{-1}$, a value typical of that observed in nearby LIRGs (e.g., Gao & Solomon 2004), but not as high as that observed in FIR-luminous, high-redshift quasar host galaxies. The star formation efficiency estimated for COserendip is also similar to that observed in two star-forming galaxies detected in CO $J = 1$–0 line emission in the outskirts of a rich galaxy cluster at $z \sim 0.4$ (Geach et al. 2009).

The specific SFR (sSFR $=$ SFR$/M_*$) is shown to follow a well-defined redshift evolution for typical star-forming galaxies, while more extreme starburst galaxies fall above this relation (e.g., Brinchmann et al. 2004; Pannella et al. 2009; Elbaz et al. 2011). In the case of the DOGs, the significant uncertainties on their SFRs prevent us from estimating stringent limits on the value of sSFR. For COserendip, the estimated stellar mass and our upper limit to the SFR implies sSFR $\leqslant 1.6$ [Gyr]$^{-1}$. This value is $\sim$3$\times$ larger than the tight relation defined by the main sequence of star-forming galaxies at $z \sim 1.1$ (Elbaz et al. 2011), potentially placing COserendip among starburst galaxies. Assuming that the upper limit to the SFR in COserendip ($\sim$150 $M_\odot$ yr^{-1}) could be maintained, its estimated molecular gas mass would be exhausted in $\sim$100 Myr, and the stellar mass would grow to $\sim 1.1 \times 10^{11}\, M_\odot$.

All of our targets show some evidence for AGN activity and are located outside the virial radii of the two clusters. Studies of the long-wavelength radio, X-ray, and thermal dust emission in active galaxies associated with massive clusters at lower redshifts have found that the number density of AGNs within the central regions of clusters increases with redshift (e.g., Galametz et al. 2009; Martini et al. 2009). Little is known about the distribution in individual objects of the molecular gas fueling this activity in intermediate-redshift ($z \sim 0.5$) cluster galaxies, and previous observations of low-J CO line emission have targeted star-forming galaxies in the process of cluster infall (Geach et al. 2009). The only exception to this is a recent detection of CO $J = 3$–2 line emission in a spiral galaxy found inside the virial radius of the cluster A370 (N. Kanekar et al., in preparation). However, this galaxy does not appear to contain an AGN, and so our detection of CO line emission in COserendip at $z \sim 1$ provides the only clear evidence for cold molecular gas in infrared-luminous AGNs associated with overdense cluster environments.

6. SUMMARY

We present the first observations of cold molecular gas, as traced by CO $J = 2$–1 line emission, in members of massive ($>10^{14}\, M_\odot$) galaxy clusters at $z \sim 1$. Despite their significant estimated infrared luminosities, two ULIRGs are not detected in CO line emission, implying cold molecular gas masses $M_{\rm H_2} \lesssim 5 \times 10^9\, M_\odot$. Given the presence of AGNs in these DOGs, which contributes to the dust heating, estimates of their star formation efficiencies are highly uncertain, and our non-detections of CO line emission are not sensitive enough to determine if these objects deviate from the $L_{\rm FIR}$–$L'_{\rm CO}$ relation. We detect CO $J = 2$–1 line emission in a third cluster member, implying a molecular gas mass of $M_{\rm H_2} = (1.55 \pm 0.28) \times 10^{10}\, M_\odot$. Contrary to the local universe where galaxy clusters are passively evolving, our detection of CO line emission in COserendip provides the first evidence for the existence of cold molecular gas in a $z \sim 1$ cluster member, demonstrating that fuel can be available in the outskirts of clusters to drive active star formation or AGN activity.

We thank Jan-Martin Winters, Melanie Krips, and Roberto Neri for their helpful advice and guidance with the data analysis. For their contributions to this survey, we thank Anthony Gonzalez and Thomas Soifer, as well as Adam Stanford for the LRIS spectrum. This work was co-funded under the Marie Curie Actions of the European Commission (FP7-COFUND). Some of the data presented herein were obtained at the W. M. Keck Observatory, which is operated as a scientific partnership among the California Institute of Technology, the University of California, and the National Aeronautics and Space Administration. The Observatory was made possible by the generous financial support of the W. M. Keck Foundation. Part of this work is based on observations made with the *Spitzer Space Telescope*, which is operated by the Jet Propulsion Laboratory, California Institute of Technology under a contract with NASA. Support for this work was provided by NASA. *Herschel* is an ESA space observatory with science instruments provided by European-led Principal Investigator consortia and with important participation from NASA.

REFERENCES

Aravena, M., Carilli, C., Daddi, E., et al. 2010, ApJ, 718, 177
Ashby, M. L. N., Stern, D., Brodwin, M., et al. 2009, ApJ, 701, 428
Bouché, N., Cresci, G., Davies, R., et al. 2007, ApJ, 671, 303
Brinchmann, J., Charlot, S., White, S. D. M., et al. 2004, MNRAS, 351, 1151
Brodwin, M., Brown, M. J. I., Ashby, M. L. N., et al. 2006, ApJ, 651, 791
Brodwin, M., Dey, A., Brown, M. J. I., et al. 2008, ApJ, 687, L65
Brodwin, M., Stern, D., Vikhlinin, A., et al. 2011, ApJ, 732, 33
Bruzual, G., & Charlot, S. 2003, MNRAS, 344, 1000
Bussmann, R. S., Dey, A., Armus, L., et al. 2012, ApJ, 744, 150
Carilli, C. L., Hodge, J., Walter, F., et al. 2011a, ApJ, 739, L33
Carilli, C. L., Walter, F., Riechers, D., et al. 2011b, arXiv:1105.1128
Carilli, C. L., & Wang, R. 2006, AJ, 131, 2763
Chabrier, G. 2003, PASP, 115, 763
Combes, F., Young, L. M., & Bureau, M. 2007, MNRAS, 377, 1795
Cooper, M. C., Newman, J. A., Weiner, B. J., et al. 2008, MNRAS, 383, 1058
Daddi, E., Dannerbauer, H., Elbaz, D., et al. 2008, ApJ, 673, L21
Dannerbauer, H., Daddi, E., Riechers, D. A., et al. 2009, ApJ, 698, L178
Desai, V., Soifer, B. T., Dey, A., et al. 2009, ApJ, 700, 1190
Dey, A., Soifer, B. T., Desai, V., et al. 2008, ApJ, 677, 943
Downes, D., & Solomon, P. M. 1998, ApJ, 507, 615
Eisenhardt, P. R. M., Brodwin, M., Gonzalez, A. H., et al. 2008, ApJ, 684, 905
Elbaz, D., Daddi, E., Le Borgne, D., et al. 2007, A&A, 468, 33
Elbaz, D., Dickinson, M., Hwang, H. S., et al. 2011, A&A, 533, A119
Elston, R. J., Gonzalez, A. H., McKenzie, E., et al. 2006, ApJ, 639, 816
Fiore, F., Grazian, A., Santini, P., et al. 2008, ApJ, 672, 94
Frayer, D. T., Harris, A. I., Baker, A. J., et al. 2011, ApJ, 726, L22
Galametz, A., Stern, D., Eisenhardt, P. R. M., et al. 2009, ApJ, 694, 1309
Gao, Y., & Solomon, P. M. 2004, ApJ, 606, 271
Geach, J. E., Smail, I., Coppin, K., et al. 2009, MNRAS, 395, L62
Greve, T. R., Bertoldi, F., Smail, I., et al. 2005, MNRAS, 359, 1165
Haines, C. P., Smith, G. P., Pereira, M. J., et al. 2010, A&A, 518, L19
Hilton, M., Lloyd-Davies, E., Stanford, S. A., et al. 2010, ApJ, 718, 133
Jannuzi, B. T., & Dey, A. 1999, in ASP Conf. Ser. 191, Photometric Redshifts and the Detection of High Redshift Galaxies, ed. R. Weymann, L. Storrie-Lombardi, M. Sawicki, & R. Brunner (San Francisco, CA: ASP), 111
Jee, M. J., Dawson, K. S., Hoekstra, H., et al. 2011, ApJ, 737, 59
Kauffmann, G., White, S. D. M., Heckman, T. M., et al. 2004, MNRAS, 353, 713
Kennicutt, R. C., Jr. 1998, ARA&A, 36, 189
Lewis, I., Balogh, M., De Propris, R., et al. 2002, MNRAS, 334, 673
Martini, P., Sivakoff, G. R., & Mulchaey, J. S. 2009, ApJ, 701, 66
Narayanan, D., Dey, A., Hayward, C. C., et al. 2010, MNRAS, 407, 1701
Nesvadba, N. P. H., Neri, R., De Breuck, C., et al. 2009, MNRAS, 395, L16
Oliver, S. J., Wang, L., Smith, A. J., et al. 2010, A&A, 518, L21
Pannella, M., Carilli, C. L., Daddi, E., et al. 2009, ApJ, 698, L116
Polletta, M., Tajer, M., Maraschi, L., et al. 2007, ApJ, 663, 81
Riechers, D. A., Capak, P. L., Carilli, C. L., et al. 2010, ApJ, 720, L131

Riechers, D. A., Walter, F., Carilli, C. L., et al. 2006, ApJ, 650, 604
Solomon, P. M., & Barrett, J. W. 1991, in IAU Symp. 146, Dynamics of Galaxies and Their Molecular Cloud Distributions, ed. F. Combes & F. Casoli (Cambridge: Cambridge Univ. Press), 235
Solomon, P. M., Downes, D., Radford, S. J. E., & Barrett, J. W. 1997, ApJ, 478, 144
Solomon, P. M., & Vanden Bout, P. A. 2005, ARA&A, 43, 677
Spergel, D. N., Bean, R., Doré, O., et al. 2007, ApJS, 170, 377
Stanford, S. A., Eisenhardt, P. R., Brodwin, M., et al. 2005, ApJ, 634, L129
Stern, D., Eisenhardt, P., Gorjian, V., et al. 2005, ApJ, 631, 163
Tran, K.-V. H., Papovich, C., Saintonge, A., et al. 2010, ApJ, 719, L126
Villar-Martín, M., Humphrey, A., Martínez-Sansigre, A., et al. 2008, MNRAS, 390, 218
Wang, R., Carilli, C. L., Neri, R., et al. 2010, ApJ, 714, 699